Two-photon-excited fluorescence of CO

Experiments and modeling

Ruchkina, Maria; Ding, Pengji; Aldén, Marcus; Bood, Joakim; Brackmann, Christian

Published in:
Optics Express

DOI:
10.1364/OE.27.025656

2019

Document Version:
Publisher's PDF, also known as Version of record

Research Article | Vol. 27, No. 18 / 2 September 2019 / Optics Express 25656
Optics EXPRESS

Two-photon-excited fluorescence of CO: experiments and modeling

MARIA RUCHKINA, PENGJI DING, MARCUS ALDÉN, JOAKIM BOOD, AND CHRISTIAN BRACKMANN*

Division of Combustion Physics, Lund University, P.O. Box 118, SE-221 00 Lund, Sweden
**christian.brackmann@forbrf.lth.se*

Abstract: A model based on rate-equation analysis has been developed for simulation of two-photon-excited laser-induced fluorescence of carbon monoxide (CO) in the Hopfield-Birge band at 230 nm. The model has been compared with experimental fluorescence profiles measured along focused beams provided by lasers emitting nano-, pico-, and femtosecond pulses. Good quantitative agreement was obtained between simulations and experimental data obtained in premixed CH_4/C_2H_4-air flames. For excitation with femtosecond pulses, experimental and simulated fluorescence signals showed quadratic dependence on laser power under conditions of low laser irradiance, whereas different sublinear dependencies were obtained at higher irradiances due to photoionization. Simulations of CO signal versus femtosecond laser linewidth suggest the strongest signal for a transform-limited pulse, which is sufficiently broad spectrally to cover the CO Q-branch absorption spectrum. Altogether, the developed rate-equation model allows for analysis of two-photon excitation fluorescence to arrange suitable diagnostic configurations and retrieve quantitative data for CO as well as other species in combustion, such as atomic oxygen and hydrogen.

1. Introduction

Carbon monoxide (CO) is an undesirable harmful combustion pollutant with strict regulations on emission levels. As a product of incomplete oxidation of carbon-based fuels, CO is a major component, 30-60%, in syngas produced via gasification, either for use as a fuel or for synthesis of chemicals [1]. In combustion, CO reportedly has impact on soot formation via flame temperature, promotion of particle surface growth and reduction of soot oxidation [2]. Ultimately, the reaction $CO + OH = CO_2 + H$ accounts for a large part of combustion heat release [3]. Efforts to accomplish a sustainable energy supply have included increased utilization of biomass-derived renewable fuels of more complex chemical composition, for which CO is a key intermediate combustion species. For example, CO is formed as an intermediate in the decomposition of alcohols [4]. Thus, CO is a key species in combustion as well as other thermochemical conversion processes and accurate measurements are of utmost importance for understanding these processes.

Among optical methods for non-invasive measurements of CO, line-of-sight absorption techniques, such as tunable diode laser absorption spectroscopy (TDLAS) [5,6], can offer sensitive detection. Measurements with high spatial and temporal resolution can be achieved with methods such as Raman spectroscopy and laser-induced fluorescence (LIF). While powerful lasers and arrangements with multiple passages of the laser beam have improved the sensitivity of Raman spectroscopy [7], the LIF method still offers better sensitivity. However, electronic resonances probed in LIF excitation of CO are located in the vacuum ultraviolet (VUV) spectral region at wavelengths below 200 nm, which are absorbed by the atmosphere and therefore rules out excitation based on absorption of a single photon. Excitation of species with VUV resonances can instead be achieved by means of two-photon absorption and this concept has allowed for LIF measurements of a range of combustion-relevant species such as CO [8,9], NH_3 [10] and atomic radicals like H [11,12], N [13], O [14] and C [15]. However, the lower cross-section of

#357453 https://doi.org/10.1364/OE.27.025656
Journal © 2019 Received 11 Jan 2019; revised 8 Jul 2019; accepted 17 Jul 2019; published 26 Aug 2019

Optics EXPRESS

two-photon absorption compared with single-photon absorption requires higher laser irradiance and pulse energies for detectable signals. The utilization of high pulse energies in turn introduces potential photo-chemical interference effects such as losses due to photoionization, formation of the probed atom or molecule via photolysis of other species, or formation of chemical species that emit interfering fluorescence. For example, laser-induced photodissociation of CO_2 into CO at high temperature has been reported to result in false positive CO fluorescence signal [16]. Moreover, emission from excited C_2 radicals formed via laser photolysis [17] has been reported to interfere with CO fluorescence [18].

While combustion diagnostics to a large extent is based on lasers emitting pulses of nanosecond duration, technical development during the last decades has resulted in an increasing number of available models operating with shorter pulses in the pico- or femtosecond regime [19]. Using such short pulses for excitation, high irradiance levels can be achieved at low pulse energies, providing efficient two-photon excitation while limiting interference from photochemistry and/or photoionization. For example, comparisons between nanosecond and picosecond excitation for fluorescence of atomic species H and O have demonstrated reduced photochemical interference using short-pulse excitation [11,12,14]. For CO, a comparison between two-photon excitation with pico- and nanosecond pulses showed that the shorter pulses resulted in less severe interferences from photolytically produced C_2 due to lower pulse energies employed for excitation [18]. Two-photon excitation of CO with femtosecond pulses has also proven beneficial in terms of low C_2 interferences for measurements in sooting flames [20,21].

Accurate interpretation and quantification of CO LIF signals require understanding of the excitation process as well as potential interfering processes. Recent studies related to this include investigations of impact of high temperature and pressure on the signal [22] and a theoretical analysis of the impact of pulse duration [23]. A model describing the CO fluorescence process under different experimental conditions would be highly valuable to identify optimum diagnostic arrangement and for retrieval of quantitative CO concentrations. With this objective in mind, a theoretical model for two-photon-excitation fluorescence of CO is presented in this paper. The model is compared with experimental data measured in premixed CH_4/C_2H_4 flames using laser pulses in the nano- (ns), pico- (ps) and femtosecond (fs) regimes. Discussion includes the ability of the model to predict CO fluorescence signals, dependence of the CO fluorescence signal on laser irradiance, effects of photoionization and laser pulse characteristics in the spectral and temporal domains.

2. Materials and methods

2.1. Laser-induced fluorescence measurements

Two-photon laser-induced fluorescence (LIF) measurements of CO were made using three different laser systems providing pulses in the ns, ps and fs regimes. Excitation with ns laser pulses was carried out using a Nd:YAG and dye laser system (Quanta-Ray PRO 250-10, Spectra Physics and Cobra Stretch-G-2400, Sirah) operating at 10 Hz repetition rate and delivering laser pulses with 8 ns duration. The dye laser was operated with LDS698 dye. Frequency-mixing between the fundamental and frequency-doubled outputs resulted in an output laser beam at 230 nm for excitation of the Q(10) line in the $B^1\Sigma^+ \leftarrow X^1\Sigma^+(0,0)$ transition of CO. The laser linewidth was specified to ~0.1 cm^{-1} and the output pulse energy was 7 mJ. Excitation with ps laser pulses was achieved using a mode-locked Nd:YAG laser (Ekspla PL 2143 C) with external amplifier (Ekspla APL70-1100). The third harmonic at 355 nm was used to pump an Optical Parametric Generator (OPG, Ekspla PG 401-P80-SH), which was tuned to wavelength 230 nm for two-photon excitation of CO. The laser pulse repetition rate was 10 Hz, the pulse duration 80 ps, the linewidth ~15 cm^{-1} and the pulse energy 400 μJ. Excitation with fs pulses was obtained with a system comprised of a Nd:YAG pump laser (Innolas), a diode-pumped mode-locked Ti:Sapphire laser (Coherent, Vitesse 2W), a Ti:Sapphire amplifier with pulse stretcher and

Optics EXPRESS

compressor (Coherent, Hidra-50-F), an optical parametric amplifier (OPA HE-TOPAS, Light Conversion) and a frequency-mixing NirUVis unit. At the wavelength 230 nm, the fs laser system delivers 125-fs pulses at 10 Hz repetition rate with maximum pulse energy of 90 μJ and beam diameter of approximately 7.5 mm. The fs laser linewidth was estimated to 200 cm^{-1}.

The laser beam was focused at the center of a porous plug burner, 10 mm above the burner surface, using spherical lenses of focal lengths f = 100 mm (ps measurements) or f = 300 mm (ns/fs measurements). Fluorescence of the CO $A^1\Pi \leftarrow B^1\Sigma^+$ transition is emitted in the visible regime and was imaged perpendicularly to the laser beam. For measurements with ns and fs laser pulses this was made using an intensified CCD camera (PI-MAX II/PI-MAX IV, Princeton Instruments) equipped with a camera lens (Nikkor f = 50 mm, $f_{\#}$=1.2, Nikon). The camera lens provided efficient suppression of the 230 nm excitation wavelength and therefore no additional detection filter was necessary. Images of the fluorescence induced along the laser beam were acquired by averaging of multiple laser pulses. A CO fluorescence emission spectrum was acquired with fs excitation having the CCD detector combined with an f = 500 mm spectrometer (Acton SpectraPro 2500, Princeton Instruments) and the signal was then collected using an f = 60 mm, $f_{\#}$=1.2 UV condenser lens. For excitation with ps laser pulses, the fluorescence was imaged using two spherical lenses (f = 200 mm and f = 37 mm) on the horizontal slit of an f = 150 mm spectrometer (Acton SpectraPro 150, grating 300 grooves/mm) connected to an iCCD camera (PI-MAX III, Princeton Instruments). In addition to the fluorescence measurements, Rayleigh scattering measurements were made in air at ambient conditions for calibration of the detector response, i.e. to convert the registered signal in detector counts into a number of photons. For the ns laser system Rayleigh scattering measurements were made using wavelength 230 nm while 520 nm, easily accessible with the tunable OPA device, was used for the measurements with the fs laser. Rayleigh scattering cross sections were obtained from Miles et al. [24].

2.2. Burner and flame conditions

Measurements were made in premixed flames stabilized on a water-cooled stainless steel porous-plug burner (Holthuis & Associates). Flows of fuel, CH_4 for ns/fs measurements and C_2H_4 for ps measurements, and air were set by mass flow controllers (Bronkhorst) with a total reactant flow of 10 l/min. A steel disc mounted above the burner surface provided a stagnation plane for further stabilization. For methane combustion, measurements were made in flames of equivalence ratios Φ=0.8, 1.0, 1.2 and 1.4 while the C_2H_4-air flame had equivalence ratio Φ=1.6.

2.3. Combustion modeling

Simulations were carried out using the stagnation plane module in CHEMKIN-PRO [25] with the AramcoMech2.0 mechanism [26], including multicomponent diffusion transport as well as thermal diffusion. The parameters GRAD = 0.5 and CURV = 0.02 resulted in a grid of ~800 points. Modelling was carried out with temperature profiles obtained by solution of the gas energy equation.

2.4. Spectral simulations

Simulations of spectra for the Q-branch of the $B^1\Sigma^+ \leftarrow X^1\Sigma^+$ (0,0) and (1,1) transitions, employed for CO excitation, and the fluorescence emission band of the $A^1\Pi \leftarrow B^1\Sigma^+$ transition were made using the PGOPHER software [27]. Rotational constants for CO were obtained from George et al. for the ground state [28], Eidelsberg et al. for the B-state [29] and Qin et al. for the A-state [30].

2.5. Fluorescence signal modeling

Spatial profiles of the two-photon fluorescence signal were simulated by a model based on four energy levels as illustrated in Fig. 1.

Optics EXPRESS

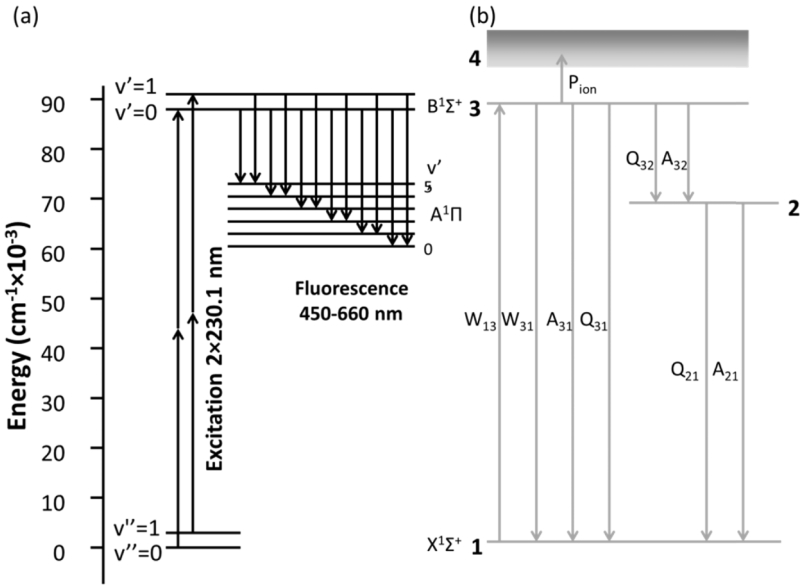

Fig. 1. Energy level diagrams for CO two-photon fluorescence. a) With optical transitions and wavelengths. b) With rate quantities for modeling.

With the populations of the four levels denoted N_1, N_2, N_3 and N_4, the following rate equations were set up for the dynamics of the system

$$\begin{aligned}
\frac{dN_1}{dt} &= -W_{13}N_1 + (Q_{21} + A_{21})N_2 + (W_{31} + Q_{31} + A_{31})N_3 \\
\frac{dN_2}{dt} &= -(Q_{21} + A_{21})N_2 + (Q_{32} + A_{32})N_3 \\
\frac{dN_3}{dt} &= W_{13}N_1 - (W_{31} + Q_{31} + A_{31} + Q_{32} + A_{32} + P_{ion})N_3 \\
\frac{dN_4}{dt} &= P_{ion}N_3
\end{aligned} \tag{1}$$

In the equations above, W_{13} represents the two-photon absorption rate whereas W_{31} is the rate for stimulated emission transitions from the excited state to the ground state. The quantities Q_{ij} represent rates for non-radiative transitions, i.e. collisional quenching, between levels labeled i and j (cf. Fig. 1). Rates of transitions resulting in spontaneous emission, i.e. fluorescence, are given by quantities A_{ij} and the rate of photoionization from the excited B-state is given by P_{ion}. In addition to these processes, stimulated emission induced via transitions from the B- to the A-state has also been reported for CO but found to be negligible at atmospheric pressure [31] and therefore not included in this model.

The rate for two-photon absorption has been determined using Eq. (2) obtained from the theory presented by Fiechtner and Gord [32].

$$W_{13} = 2\sigma_0{\phi_0}^2 G^{<2>}\Gamma^{<2>} \tag{2}$$

In Eq. (2) σ_0 is the integrated cross section for two-photon absorption and Φ_0 is the integrated flux of the laser i.e. the number of photons per area and time unit. The factor $G^{<2>}$ is the second-order intensity correlation function at zero delay and has in these simulations been set equal to one, which is the theoretical value assumed for coherent light sources. The overlap

Optics EXPRESS

between the laser line profile and the CO absorption spectrum line shape is given by the factor $\Gamma^{<2>}$, which is calculated according to Eq. (3) [32].

$$\Gamma^{<2>} = \int_{-\infty}^{\infty}\int_{-\infty}^{\infty} f(\nu_1)f(\nu_2)g(\nu_1+\nu_2)d\nu_1 d\nu_2 \tag{3}$$

The normalized spectral line shape of the laser radiation and the CO species is given by functions f(ν) and g(ν), respectively. The two-photon absorption cross section σ_0=1.5·10^{-35} cm^4 has been obtained from DiRosa and Farrow [33]. Rates for spontaneous emission, A_{ij}, have been obtained from works by Qin et al. [30] while collisional quenching rates Q_{ij}, have been determined from cross section data presented by Settersten et al. [34].

The photoionization rate, P_{ion}, is given by Eq. (4)

$$P_{ion} = \sigma_{ion}\phi_0 \tag{4}$$

The value of the photoionization cross section determined by Di Rosa & Farrow, σ_{ion}=10·10^{-18} cm^2 [35], was employed in the model. The photon flux, Φ_0, is dependent on the laser beam cross section area and thus the beam diameter, which is modeled using Eq. (5) for a so-called embedded Gaussian beam.

$$d(z) = Md_0\sqrt{1+\left(\frac{\lambda z}{\pi\left(\frac{d_0}{2}\right)^2}\right)^2} \tag{5}$$

For a Gaussian beam the diameter is defined according to the distance where the intensity is a factor $1/e^2 = 0.14$ of the maximum value. In Eq. (5) λ is the laser wavelength, z is the distance from the beam focus, M is the laser beam propagation constant and d_0 is the diameter of the ideal Gaussian beam. For positions along a focused laser beam, the beam diameter, laser photon flux, ionization rate, and two-photon absorption rate can be determined according to Eq. (2)–(5) and be used as input for the differential equations in Eq. (1). These differential equations can then be solved for populations N_1, N_2, N_3 and N_4 with the initial value for N_1 given by the CO concentration of the gas.

3. Results

3.1. CO two-photon fluorescence spectroscopy

Figure 2 shows the CO two-photon fluorescence signal versus excitation wavelength, i.e. excitation spectra. For excitation using the narrowband (~0.1 cm^{-1}) ns laser, the spectrum of Fig. 2(a) shows the Q-branch of the $B^1\Sigma^+ \leftarrow X^1\Sigma^+(0,0)$ Hopfield-Birge band with partially resolved rotational structure. The experimental spectrum (top) is well represented by a simulation (bottom) for temperature 1700K obtained using the PGOPHER software. At 229.98 nm the experimental spectrum shows a dip indicated by an arrow in the figure and not predicted by the simulation. This feature has also been observed by Carrivain et al. and assigned to originate from ionization of CO [22,36]. For measurement of CO profiles the ns laser was tuned to 229.98 nm, mainly probing the Q(10) transition. Excitation using the spectrally much broader fs laser pulses results in a spectrum without any resolved detail, presented with circle symbols in Fig. 2(b). A Gaussian profile that fits the measured data points can be obtained by introducing a ~350 cm^{-1} wide (FWHM) Gaussian instrument function for the simulated CO spectrum, as displayed by the solid line profile in Fig. 3b. The width of the fitted two-photon excitation profile represents a convolution of the laser spectral profile with the profile itself (cf. Eq. (3)) and in turn with the CO absorption spectrum. The resulting profile from the convolution of the laser profile with itself

Optics EXPRESS

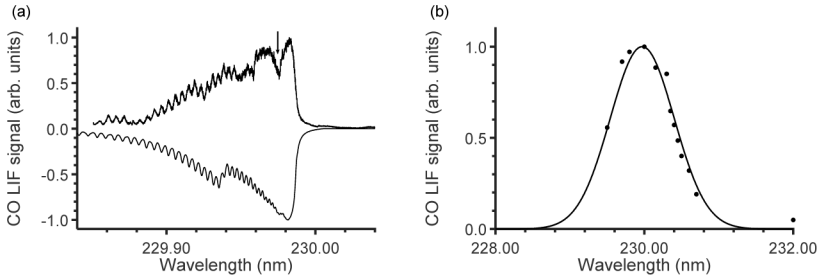

Fig. 2. Fluorescence excitation spectra with a) ns laser excitation and b) fs laser excitation. In a) experimental data are shown at the top and a PGOPHER simulation is for clarity shown with negative intensity below. In b) experimental data are shown with circles and a PGOPHER simulation with solid line.

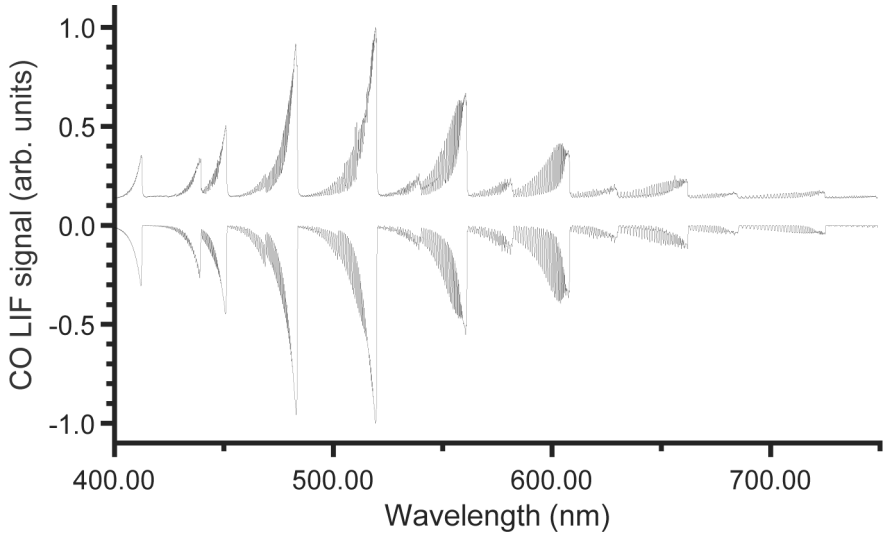

Fig. 3. CO fluorescence emission spectra with vibrational bands of the $A^1\Pi \leftarrow B^1\Sigma^+$ transition. Spectrum obtained with fs laser excitation in CH_4-air flame (top) and from PGOPHER simulation at temperature 1700K (bottom). The strengths of vibrational bands in the simulated spectrum have been adjusted to match the experimental data and the spectrum has been plotted with negative intensities for easier comparison in the plot.

will be a factor 1.4 broader. Also considering the width of the CO Q-branch suggests the laser linewidth to be ~200 cm^{-1}. For measurements of spatial CO profiles, the fs laser wavelength was set to the value resulting in maximum signal, i.e. positioned at 230.00 nm.

Figure 3 shows a CO fluorescence emission spectrum obtained for fs laser excitation in a CH_4-air flame of equivalence ratio Φ=1.4 (top) together with a spectrum obtained from a PGOPHER simulation (bottom) at temperature 1700K. The simulated spectrum has been plotted with negative intensities to assist comparison in the plot.

Vibrational bands with partially resolved rotational structure are observed for the $A^1\Pi \leftarrow B^1\Sigma^+$ transition. Compared with excitation using ns or ps laser [18], the spectrum of Fig. 3 shows additional emission bands, which was also observed by Li et al. [23] and Rahman et al. [37]. Compared with ns and ps lasers the fs pulses are sufficiently broad spectrally, to also allow for excitation of the (1-1) band of the $B^1\Sigma^+ \leftarrow X^1\Sigma^+$ transition resulting in additional emission bands corresponding to transitions from the v = 1 level of the B-state. The strengths of the

Optics EXPRESS

vibrational bands in the simulated spectrum have been adjusted to match the experimental data, thus accounting for differences in detection sensitivity for different wavelengths. Detailed studies of the spectra show some mismatch, up to 0.06 nm, in positions of rotational lines that potentially could be due to inaccuracies introduced during scanning of the spectrometer over the wide wavelength range. Nevertheless, all the emission bands are well predicted by the simulated spectrum, thus confirming the fluorescence detected with fs laser excitation to be generated by CO. Characterization of the CO excitation spectrum and the fluorescence emission bands as presented in Figs. 2 and 3 provided necessary input for modeling of the two-photon-excitation fluorescence, such as estimations of the laser spectral width and information on which fluorescence emission bands to include in the A_{32} constant of the rate-equation model (cf. Eq. (1)).

3.2. CO fluorescence profiles

Figure 4 shows CO fluorescence profiles measured with ns (Figs. 4(a), 4(c) and 4(e)) and fs laser excitation (Figs. 4(b),4(d) and 4(f)) for CH_4-air flames of equivalence ratios Φ=1.4, 1.2 and 1.0.

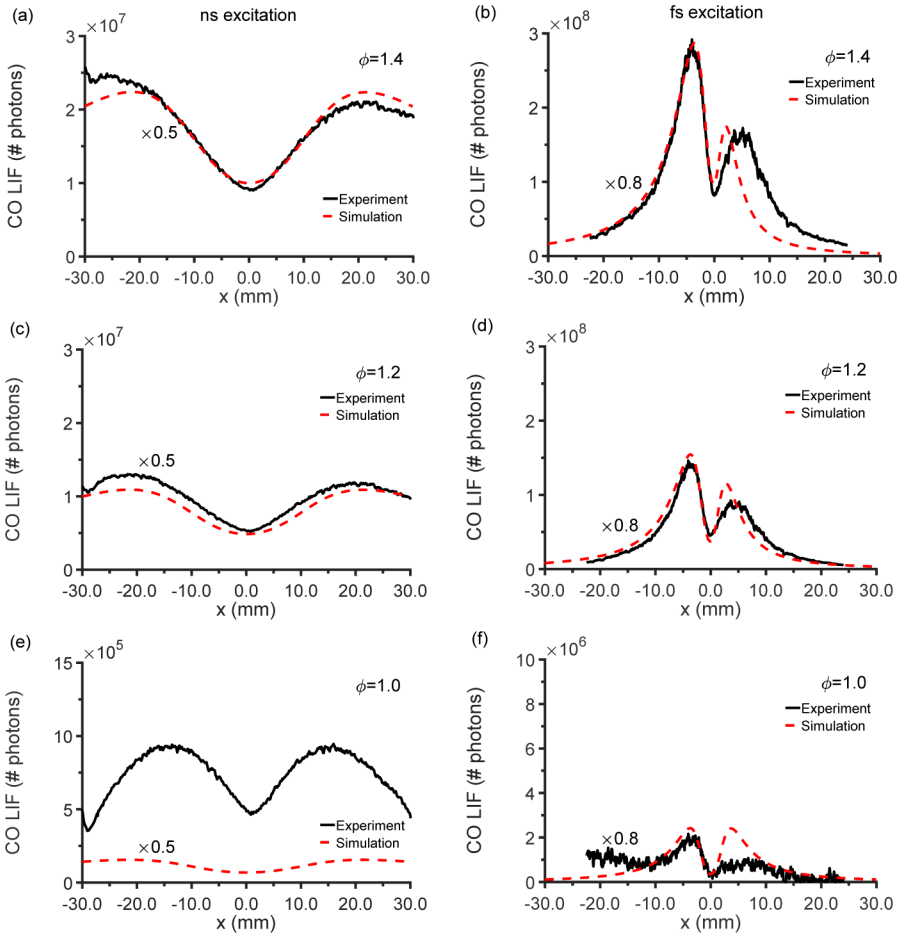

Fig. 4. Experimental (solid black lines) and modeled (dashed red lines) CO fluorescence profiles for CH_4-air flames for equivalence ratios Φ=1.4, 1.2 and 1.0 with ns laser (a,c,e) and fs laser (b,d,f) excitation. The laser beam propagates from left to right and is focused at position x = 0 mm. Absorption results in asymmetric profiles and ionization at the beam focus introduces a loss mechanism and decreased signal. Further details are given in the Results section.

Optics EXPRESS

The results were obtained with high energy of 7 mJ for the long ns pulses and with low energy of 10 μJ for the short fs pulses. In the latter case, energies higher than ~10 μJ resulted in dielectric breakdown in the beam focus, setting an upper limit for the pulse energy employed when focusing using the f = 300 mm lens. In the figures the laser beam propagates from left to right and is focused at position x = 0 mm. For this type of flames, uniform conditions are expected at a specific height above the burner, and thus the CO concentration is constant along the laser beam path. Moreover, the CO concentration remains rather constant versus height in the flame product zone as chemical equilibrium has been established. For example, fs laser measurements at heights 2-10 mm in the Φ=1.4 flame showed CO signal variations of 10% or less. With constant concentration, the observed variations in signal along the beam path are related to the non-uniform irradiance distribution along the beam and the interactions between the laser photons and CO molecules.

Propagation of the laser beam through the uniform CO distribution results in two-photon absorption and thus lower excitation efficiency at the right side of the profiles and accounts for the asymmetry observed. The two-photon absorption is proportional to the square of the laser irradiance and an increase in signal can be observed following the profiles from the outer edges towards the center. In addition, the deep-UV laser induces photoionization of CO along the beam path, which depends linearly on the laser irradiance and results in a loss of excited CO molecules and thus fluorescence signal. In the vicinity of the beam focus, x = 0 mm, photoionization supersedes two-photon absorption resulting in signal decrease, manifested by a dip in the profiles. This trend is observed in experiments as well as simulations, for both ns and fs excitation in the Φ=1.4 and Φ=1.2 flames as well as in the experimental profile of Fig. 4(e) acquired with ns laser excitation in the stoichiometric (Φ=1.0) flame. The exact shape of the profile is determined by the laser beam focusing geometry determined by the beam size and divergence properties. Comparing experimental profiles for ns and fs excitation in Fig. 4 it is evident that the laser beams foci are different even though both beams were focused with f = 300 mm lenses. In general, tighter focusing result in closer spaced peaks and a more pronounced dip due to photoionization. These trends for two-photon fluorescence have been observed previously and analyzed qualitatively [38].

As seen in Figs. 4(a)–4(d), the simulations presented with the dashed red profiles readily capture the experimental profile shapes, shown in with solid black lines, for the fuel-rich Φ=1.4 and Φ=1.2 flames as well as for measurements in the stoichiometric flame (Fig. 4(f)). A mismatch in shape can be observed on the left side of the profiles in Fig. 4(a) where the experimental profile shows higher values than simulations while the rest of profile shows better agreement. A possible reason for this could be a decrease in temperature at the edge of flame resulting in a locally higher number density not accounted for in the simulations. Quantitatively, simulations and experiments show good agreement considering the model complexity. Nevertheless, simulations generally over predicted signals and have been multiplied by factors 0.5 or 0.8, indicated in the graphs, for comparison with experimental data in Fig. 4. The consistent over prediction and similar magnitude of these factors indicate that a common source could account for part of the discrepancy, possibly related to uncertainties in quantities employed in the model, for example the cross sections for two-photon absorption and photoionization. The fluorescence signal simulated for fs excitation in the rich Φ=1.4 (Fig. 4(b)) and Φ=1.2 (Fig. 4(d)) flames is approximately one order of magnitude higher than that for ns laser excitation (Figs. 4a and c), The ratio between the signals of the Φ=1.4 and Φ=1.2 flames is 1.9 and 2 for ns and fs laser excitation, respectively. This is consistent with the decrease in CO concentration from 6.1% to 3.0% obtained from flame chemistry simulations.

For the stoichiometric flame, chemistry simulations give a CO concentration of 0.043% which is a factor of 67 lower than the concentration of the Φ=1.2 flame. For fs laser excitation the fluorescence signal shows a corresponding decrease by a factor of 75 whereas for ns laser

Optics EXPRESS

excitation the signal is merely reduced by a factor of 14. For the latter case the measured signal is thus higher than expected, which can be explained by production of CO via laser-induced photolysis of CO_2 resulting in a false positive CO signal, as reported by Nefedov et al. [15]. In their work, the level of photolytically produced CO is suggested to amount to about 3% of the CO_2 concentration. For the stoichiometric flame, the CO_2 concentration of the product gas is 9%, which by photolysis would result in additional CO of 0.27%. Adding a contribution of this magnitude due to photolysis gives an apparent CO concentration of 0.31%. The decrease from 3.0% to 0.31% corresponds to a factor 10 and is in better consistency with the factor 14 observed for the ns experimental data. Moreover, the shape of the profile measured with ns laser excitation in the Φ=1.0 flame is different from that observed for the rich flames. This suggest a different dependence on laser irradiance and the impact of another process such as photolysis. Further indication of CO_2 photolysis for ns laser excitation was obtained from measurements in a lean Φ=0.8 flame (data not shown), which resulted in a CO signal of ~$1.8{\cdot}10^6$ photons, i.e. 35% lower than that of the stoichiometric flame, even though the calculated CO concentration of the Φ=0.8 flame is 15 ppm. In contrast, fs laser excitation in the Φ=0.8 flame did not generate any observable CO signal, indicating that CO two-photon fluorescence can be measured free from photolytic interferences with fs laser excitation as presented by Wang and Kulatilaka [20,21]. Richardson et al. have reported that CO measurements with minimal photolytic interferences, for example by dissociation of CO_2, can be achieved for fs excitation provided that the laser intensity is kept below 10^{10} W/cm^2 [21]. Thus, care has to be taken considering the experimental conditions in interpretation of results. If the signal obtained with ns excitation in the Φ=0.8 flame is considered to be solely originating from CO_2 photolysis and an approximate background for the stoichiometric flame, the signal of the stoichiometric flame with ns excitation would be reduced to ~$1{\cdot}10^6$ photons, which is a factor of 38 lower than the signal of the Φ=1.2 flame and more consistent with the decrease in concentration of nascent CO in the flame. Figure 5 presents CO profiles for an intermediate case, in terms of pulse duration, for excitation with ps pulses.

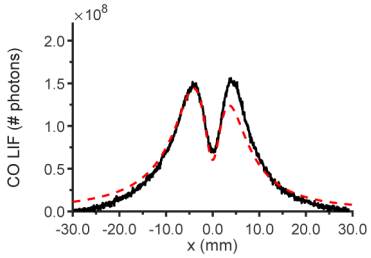

Fig. 5. Experimental (solid black line) and modeled (dashed red line) CO fluorescence profiles for a C_2H_4-air flame of equivalence ratio Φ=1.6 with ps laser excitation. The laser beam propagates from left to right and is focused at position x = 0 mm. Ionization at the beam focus introduces a loss mechanism and decreased signal.

The experimental CO fluorescence profile of Fig. 5 was measured in a premixed C_2H_4-air flame of equivalence ratio Φ=1.6 for which chemistry simulation predict a CO concentration of 11%. The shape of the simulated CO profile shows good agreement with experimental data, however, the simulation predicts an absorption with a lower second peak not observed for the measurements. The C_2H_4 flame of Φ=1.6 is approaching sooting conditions with formation of precursors, which may introduce some absorption of the laser beam resulting in reduced intensity for CO excitation, less two-photon absorption and lack of asymmetry in the experimental profile. Altogether, Figs. 4 and 5 demonstrate that the model permits good prediction of CO fluorescence profiles for different excitation laser and beam focusing alternatives.

Optics EXPRESS

As shown for the results for fs excitation in Fig. 4, two-photon absorption results in an asymmetric shape of the fluorescence profiles, which may be used to quantify the CO concentration. Figure 6(a) presents simulated CO profiles, obtained with the laser parameters used to mimic the experimental fs data in Fig. 4, for concentrations in the range 0.5–5% at temperature 1700K. A transmission parameter has been calculated for such profiles for CO concentrations in the range 0.5-10% by forming the ratio between the two peaks located on opposite sides of the focus position at 0 mm and is presented versus CO concentration in Fig. 6(b).

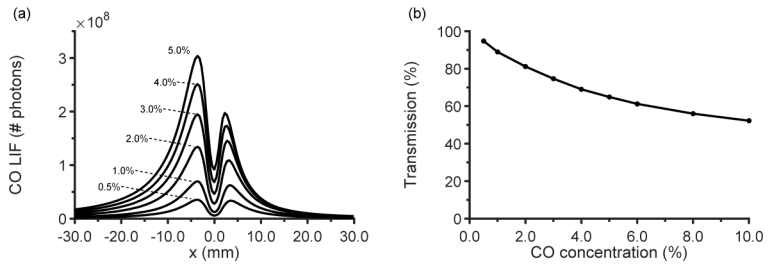

Fig. 6. a) Simulated CO fluorescence profiles for fs laser excitation at CO concentrations between 0.5 and 5% at temperature 1700 K. b) Transmission, calculated as the ratio between the LIF signal at the two peaks of the profiles, versus CO concentration. A CO concentration in the range 1-2% results in 10% reduction in peak intensity.

The profile in Fig. 6(a) with the lowest signal corresponds to a concentration of 0.5% and shows 3% reduction in signal between the left and the right peak of the profile. With increasing CO concentration, the asymmetric shape of the profiles becomes more noticeable (cf. Fig. 6(a)) and the calculated transmission factor decreases (cf. Fig. 6(b)). Individual fluorescence profiles measured with the fs laser showed variations in the transmission ratio on the order of 1%, thus a detection limit on the order of 0.5% is feasible for this experimental setup. The two-photon absorption rate has a quadratic dependence on laser irradiance (cf. Eq. (2)) and the impact of absorption on the shape of the fluorescence profiles is in many cases much less apparent for excitation using ns or ps laser pulses (cf. Figs. 4 and 5).

3.3. *Power dependence analysis*

CO fluorescence profiles for fs pulse excitation at different laser pulse energies were obtained from measurements as well as calculations and the signal power dependence was investigated. Figure 7(a) shows CO fluorescence profiles obtained for fs pulse excitation at pulse energies 3 and 8 μJ while power-dependence curves obtained for two regions along the profile are presented in Figs. 7(b) and 7(c).

The signal in a region around position −20 mm, indicated by the left arrow in Fig. 7(a), where it starts to increase as the beam propagates towards the focus, is presented in Fig. 7(b). Circle and square symbols show results from experiments and simulations, respectively, together with fitted E^n curves shown as lines on the logarithmic scale of the graph. Measured and simulated data were fitted to curves of n = 2.03 and n = 1.98, respectively. Both values are close to 2, resembling the quadratic dependence of a two-photon excitation process, which is expected since the laser beam in this region is quite diverged compared with the central region at the focus. The laser irradiance in this region is thus too low to result in any apparent signal loss due to photoionization. In contrast, in the region at the beam focus, position 0 mm indicated by the right arrow in Fig. 7(a), the profiles show a distinct dip due to photoionization. With increasing pulse energy, the depth of the dip becomes larger, meaning that increasing amounts of CO molecules in the excited B-state are photoionized. This occurs during the fs laser pulse, i.e. on a time-scale shorter than that of fluorescence, for which the lifetime is approximately 0.35 ns [39], and thus dominates over the

Optics EXPRESS

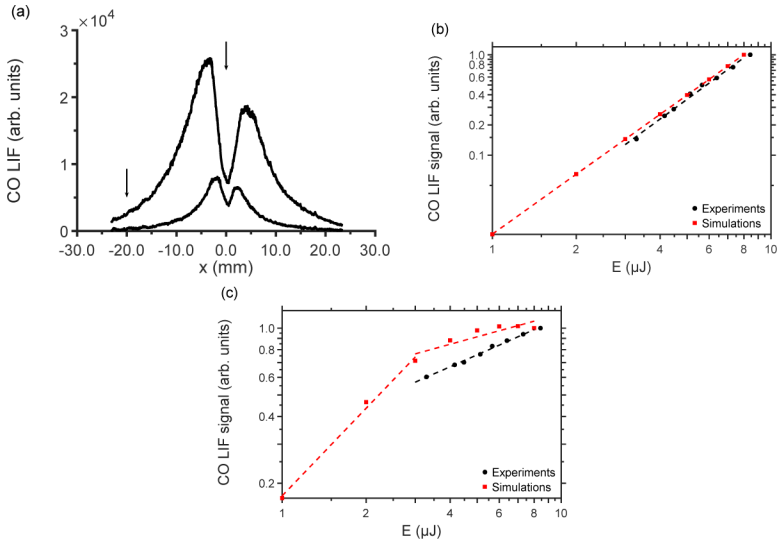

Fig. 7. a) CO fluorescence profiles for fs laser excitation at pulse energies 3 and 8 μJ. Arrows indicate regions for evaluation of signal power dependence. Signal power dependence for fs laser pulse excitation at position -20 mm (b) and at the focus (c) of the fluorescence profile. Results from experiments and simulations are shown with circle and square symbols, respectively. Signals measured at −20 mm can be fitted to lines with slopes ~2, indicating quadratic power dependence for the two-photon excitation. CO photoionization in the vicinity of the beam focus results in reduced power dependencies, slopes 0.56 and 0.35 for experiments and simulations, respectively.

quenching and influences the fluorescence data. Results of CO signal power dependence for this region are presented in Fig. 7(c) where experimental data and simulated results for pulse energies 3-8 μJ are fitted to curves of n = 0.56 and n = 0.35, respectively. The lower value of the exponent for the simulated results indicates that the photoionization effect could be overestimated relative to the two-photon absorption and subsequent fluorescence. However, there are uncertainties in the reported cross section values for two-photon absorption and photoionization [33,35], for example the photoionization cross section reported by Di Rosa & Farrow [35] is reported with an accuracy of ± 30%. Simulated results for pulse energies below 3 μJ show stronger power dependence and are fitted by a curve of n = 1.31. For all pulse energies the power dependence is lower than quadratic due to photoionization, but for values below 3 μJ the impact and loss in fluorescence signal are less severe resulting in a higher power-dependence exponent. Rahman et al. measured the power dependence of the CO LIF signal obtained for excitation with fs pulses and the laser beam focused into a mm-size sheet [37]. For intensities up to $1.7 \cdot 10^{10}$ W/cm^2 the signal followed a quadratic power dependence while data acquired at somewhat higher irradiances indicated reduced power dependence due to photoionization [37]. For the experimental data presented in Fig. 7, signal at different positions along the fluorescence profiles follow quadratic trends until position −7 mm where a decrease to an $E^{1.9}$-dependence was observed. At this position the beam diameter is estimated to 170 μm, which for a pulse of 8 μJ energy and 125 fs duration would correspond to $2.9 \cdot 10^{11}$ W/cm^2. This value is thus an order of magnitude higher than the limit presented by Rahman et al. [37]. However, accurate comparison requires detailed knowledge on the experimental conditions of both studies, in particular beam focusing and laser spot size.

According to the discussion by Settersten and Linne, rate equations, here employed for CO simulations, in general provide accurate analysis only when the laser pulse rise time is significantly longer than the characteristic dephasing time related to molecular collisions [40]. While it

Optics EXPRESS

is stated that accurate analysis instead requires density-matrix equations, the benefits of rate equations for analysis of complex systems is also recognized. In [40], Settersten and Linne also report that under conditions of strong collisional quenching, rate-equation analysis nevertheless performs well, determining the excited state population accurately also for laser pulses shorter than the dephasing time. For fs pulses the laser-induced photoionization loss mechanism clearly acts on a much shorter time-scale than collision-induced processes and rate-equation analysis might therefore have limitations in accuracy under these conditions. In particular, for the beam focus region, around position 0 mm, where photoionization is strongest. Nonetheless, the model shows excellent agreement with experimental results for position −20 mm where collisional quenching dominates and also well predicts the trends of experimental data for position 0 mm.

3.4. Linewidth analysis

The fluorescence signal is dependent on the spectral overlap between the laser and the CO two-photon absorption spectrum, represented by the factor $\Gamma^{<2>}$ in Eq. (3), and to investigate this CO fluorescence profiles were simulated for different laser linewidths assuming a pulse duration of 125 fs. The results are presented in Fig. 8 for laser linewidths ranging from 120 cm^{-1}, representing a transform-limited Gaussian pulse of 125 fs, up to 300 cm^{-1}. Strongest signal is achieved for the spectrally narrowest, transform-limited, pulse, since the fs laser spectral profile essentially covers the CO Q-branch spectrum (cf. Fig. 2) also for this smallest linewidth. For this reason, the suggestion by Li et al., that a transform-limited laser pulse provides best fs CO excitation and fluorescence signal [23], is valid even though based on a simpler analysis without considering the overlap between laser and CO absorption spectrum. In general, however, accurate simulations require the shape of the CO spectrum to be considered in the analysis.

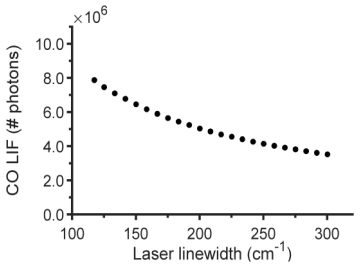

Fig. 8. Simulated CO signal dependence on fs laser linewidth. Best spectral overlap with the CO Q-branch and signal generation is obtained for the spectrally narrowest, transform-limited, pulse.

4. Conclusions

A model based on rate-equation analysis has been presented for simulating two-photon-excitation fluorescence of CO. The model has been compared with experimental fluorescence profiles measured along focused beams provided by lasers emitting ns, ps, and fs pulses. Simulated CO profiles for the product gas of premixed CH_4/C_2H_4-air flames show good quantitative agreement with experimental data for all pulse durations. Excitation with fs laser pulses shows strong signals and provides efficient CO excitation with low photochemical interferences as reported in previous works. Experimental and simulated fluorescence signals for fs-pulse excitation showed quadratic dependence on laser power under conditions of low laser irradiance, for which non-radiative depopulation of the excited state is dominated by collisional processes. At higher irradiances, obtained in the vicinity of the laser beam focus, both experiments and modeling show sublinear trends due to photoionization. A somewhat weaker dependence observed for the rate-equation

Optics EXPRESS

predictions could be due to uncertainties in cross section data or indicate a limitation of this modeling approach for rapid depopulation of the excited state by interaction with ultrashort laser pulses. Analysis using density-matrix equations may provide more accurate results. The spectral overlap between the laser and the atomic/molecular absorption line is in general a crucial quantity for accurate analysis of fluorescence signals. Altogether, the developed model can be applied to arrange suitable diagnostic configurations and for quantitative analysis of experimental data.

Funding

Energimyndigheten (38913-2 - GRECOP); Knut och Alice Wallenbergs Stiftelse (2015.0294 - ALADIN); H2020 European Research Council (669466 - TUCLA).

Acknowledgments

The authors gratefully acknowledge the initial investigations on CO fluorescence modeling carried out by M. Sc. Martin Karlsson and Mr. Ryo Sasaki.

References

1. P. J. Woolcock and R. C. Brown, "A review of cleaning technologies for biomass-derived syngas," Biomass Bioenergy **52**, 54–84 (2013).
2. H. S. Guo, K. A. Thomson, and G. J. Smallwood, "On the effect of carbon monoxide addition on soot formation in a laminar ethylene/air coflow diffusion flame," Combust. Flame **156**(6), 1135–1142 (2009).
3. J. Warnatz, U. Maas, and W.R. Dibble, *Combustion : physical and chemical fundamentals, modeling and simulation, experiments, pollutant formation* (Springer, 2006).
4. S. M. Sarathy, P. Osswald, N. Hansen, and K. Kohse-Hoinghaus, "Alcohol combustion chemistry," Prog. Energy Combust. Sci. **44**, 40–102 (2014).
5. X. Chao, J. B. Jeffries, and R. K. Hanson, "Absorption sensor for CO in combustion gases using 2.3 μm tunable diode lasers," Meas. Sci. Technol. **20**(11), 115201 (2009).
6. R. K. Hanson and D. F. Davidson, "Recent advances in laser absorption and shock tube methods for studies of combustion chemistry," Prog. Energy Combust. Sci. **44**, 103–114 (2014).
7. K. C. Utsav, J. A. Silver, D. C. Hovde, and P. L. Varghese, "Improved multiple-pass Raman spectrometer," Appl. Opt. **50**(24), 4805–4816 (2011).
8. M. Aldén, S. Wallin, and W. Wendt, "Applications of 2-Photon Absorption for Detection of CO in Combustion Gases," Appl. Phys. B: Photophys. Laser Chem. **33**(4), 205–208 (1984).
9. B. J. Kirby and R. K. Hanson, "Imaging of CO and CO_2 using infrared planar laser-induced fluorescence," Proc. Combust. Inst. **28**(1), 253–259 (2000).
10. C. Brackmann, O. Hole, B. Zhou, Z. Li, and M. Aldén, "Characterization of ammonia two-photon laser-induced fluorescence for gas-phase diagnostics," Appl. Phys. B: Lasers Opt. **115**(1), 25–33 (2014).
11. W. D. Kulatilaka, J. R. Gord, V. R. Katta, and S. Roy, "Photolytic-interference-free, femtosecond two-photon fluorescence imaging of atomic hydrogen," Opt. Lett. **37**(15), 3051–3053 (2012).
12. W. D. Kulatilaka, B. D. Patterson, J. H. Frank, and T. B. Settersten, "Comparison of nanosecond and picosecond excitation for interference-free two-photon laser-induced fluorescence detection of atomic hydrogen in flames," Appl. Opt. **47**(26), 4672–4683 (2008).
13. U. Westblom, S. Agrup, M. Aldén, and P. Cederbalk, "Detection of Nitrogen-Atoms in Flames Using 2-Photon Laser-Induced Fluorescence and Investigations of Photochemical Effects," Appl. Opt. **30**(21), 2990–3002 (1991).
14. J. H. Frank, X. L. Chen, B. D. Patterson, and T. B. Settersten, "Comparison of nanosecond and picosecond excitation for two-photon laser-induced fluorescence imaging of atomic oxygen in flames," Appl. Opt. **43**(12), 2588–2597 (2004).
15. U. Westblom, P. E. Bengtsson, and M. Aldén, "Carbon-Atom Fluorescence and C_2 Emission Detected in Fuel-Rich Flames Using a Uv Laser," Appl. Phys. B: Photophys. Laser Chem. **52**(6), 371–375 (1991).
16. A. P. Nefedov, V. A. Sinel'shchikov, A. D. Usachev, and A. V. Zobnin, "Photochemical effect in two-photon laser-induced fluorescence detection of carbon monoxide in hydrocarbon flames," Appl. Opt. **37**(33), 7729–7736 (1998).
17. J. E. M. Goldsmith and D. T. B. Kearsley, "C_2 Creation, Emission, and Laser-Induced Fluorescence in Flames and Cold Gases," Appl. Phys. B: Photophys. Laser Chem. **50**(5), 371–379 (1990).
18. C. Brackmann, J. Sjoholm, J. Rosell, M. Richter, J. Bood, and M. Aldén, "Picosecond excitation for reduction of photolytic effects in two-photon laser-induced fluorescence of CO," Proc. Combust. Inst. **34**(2), 3541–3548 (2013).
19. J. R. Gord, T. R. Meyer, and S. Roy, "Applications of Ultrafast Lasers for Optical Measurements in Combusting Flows," Annu. Rev. Anal. Chem. **1**(1), 663–687 (2008).

Optics EXPRESS

20. D. R. Richardson, S. Roy, and J. R. Gord, "Femtosecond, two-photon, planar laser-induced fluorescence of carbon monoxide in flames," Opt. Lett. **42**(4), 875–878 (2017).
21. Y. J. Wang and W. D. Kulatilaka, "Detection of carbon monoxide (CO) in sooting hydrocarbon flames using femtosecond two-photon laser-induced fluorescence (fs-TPLIF)," Appl. Phys. B: Lasers Opt. **124**(1), 8 (2018).
22. O. Carrivain, M. Orain, N. Dorval, C. Morin, and G. Legros, "Experimental Spectroscopic Studies of Carbon Monoxide (CO) Fluorescence at High Temperatures and Pressures," Appl. Spectrosc. **71**(10), 2353–2366 (2017).
23. B. Li, X. F. Li, D. Y. Zhang, Q. Gao, M. F. Yao, and Z. S. Li, "Comprehensive CO detection in flames using femtosecond two-photon laser-induced fluorescence," Opt. Express **25**(21), 25809–25818 (2017).
24. R. B. Miles, W. R. Lempert, and J. N. Forkey, "Laser Rayleigh scattering," Meas. Sci. Technol. **12**(5), R33–R51 (2001).
25. "CHEMKIN-PRO 15101," (Reaction Design, 2010).
26. Y. Li, C. W. Zhou, K. P. Somers, K. W. Zhang, and H. J. Curran, "The oxidation of 2-butene: A high pressure ignition delay, kinetic modeling study and reactivity comparison with isobutene and 1-butene," Proc. Combust. Inst. **36**(1), 403–411 (2017).
27. C. M. Western, "PGOPHER: A program for simulating rotational, vibrational and electronic spectra," J. Quant. Spectrosc. Radiat. Transfer **186**, 221–242 (2017).
28. T. George, W. Urban, and A. Lefloch, "Improved Mass-Independent Dunham Parameters for the Ground-State of CO and Calibration Frequencies for the Fundamental-Band," J. Mol. Spectrosc. **165**(2), 500–505 (1994).
29. M. Eidelsberg, J. Y. Roncin, A. Lefloch, F. Launay, C. Letzelter, and J. Rostas, "Reinvestigation of the Vacuum Ultraviolet-Spectrum of Co and Isotopic-Species - the $B^1\Sigma^+ \leftrightarrow X^1\Sigma^+$ Transition," J. Mol. Spectrosc. **121**(2), 309–336 (1987).
30. Z. Qin, J. M. Zhao, and L. H. Liu, "Radiative transition probabilities for the main diatomic electronic systems of N_2, N_2^+, NO, O_2, CO, CO^+, CN, C_2 and H_2 produced in plasma of atmospheric entry," J. Quant. Spectrosc. Radiat. Transfer **202**, 286–301 (2017).
31. U. Westblom, S. Agrup, M. Aldén, H. M. Hertz, and J. E. M. Goldsmith, "Properties of Laser-Induced Stimulated-Emission for Diagnostic Purposes," Appl. Phys. B: Photophys. Laser Chem. **50**(6), 487–497 (1990).
32. G. J. Fiechtner and J. R. Gord, "Absorption and the dimensionless overlap integral for two-photon excitation," J. Quant. Spectrosc. Radiat. Transfer **68**(5), 543–557 (2001).
33. M. D. Di Rosa and R. L. Farrow, "Two-photon excitation cross section of the B ← X(0,0) band of CO measured by direct absorption," J. Opt. Soc. Am. B **16**(11), 1988–1994 (1999).
34. T. B. Settersten, A. Dreizler, and R. L. Farrow, "Temperature- and species-dependent quenching of CO *B* probed by two-photon laser-induced fluorescence using a picosecond laser," J. Chem. Phys. **117**(7), 3173–3179 (2002).
35. M. D. Di Rosa and R. L. Farrow, "Cross sections of photoionization and ac Stark shift measured from Doppler-free B ← X(0,0) excitation spectra of CO," J. Opt. Soc. Am. B **16**(5), 861–870 (1999).
36. F. Di Teodoro and R. L. Farrow, "CO^+ $B^2\Sigma^+$ (v=0) emission induced by laser excitation of neutral CO at 230 nm," J. Chem. Phys. **114**(8), 3421–3428 (2001).
37. K. A. Rahman, K. S. Patel, M. N. Slipchenko, T. R. Meyer, Z. L. Zhang, Y. Wu, J. R. Gord, and S. Roy, "Femtosecond, two-photon, laser-induced fluorescence (TP-LIF) measurement of CO in high-pressure flames," Appl. Opt. **57**(20), 5666–5671 (2018).
38. M. Aldén, U. Westblom, and J. E. M. Goldsmith, "2-Photon-Excited Stimulated-Emission from Atomic Oxygen in Flames and Cold Gases," Opt. Lett. **14**(6), 305–307 (1989).
39. M. Jonsson, A. Ehn, M. Christensen, M. Aldén, and J. Bood, "Simultaneous one-dimensional fluorescence lifetime measurements of OH and CO in premixed flames," Appl. Phys. B: Lasers Opt. **115**(1), 35–43 (2014).
40. T. B. Settersten and M. A. Linne, "Modeling pulsed excitation for gas-phase laser diagnostics," J. Opt. Soc. Am. B **19**(5), 954–964 (2002).